Journal of Statistical Planning and Inference 140 (2010) 3597–3607

Contents lists available at ScienceDirect

Journal of Statistical Planning and Inference

journal homepage: www.elsevier.com/locate/jspi

Stochastic modeling of particle movement with application to marine biology and oceanography

David R. Brillinger [a,*], Brent S. Stewart [b]

[a] Statistics Department, University of California, Berkeley, CA 94720, USA
[b] Hubbs-SeaWorld Research Institute, 2595 Ingraham Street, San Diego, CA 92109, USA

ARTICLE INFO

Available online 16 May 2010

MSC:
primary 62M10, 60G55
secondary 62M99, 91B30

Keywords:
Functional stochastic differential equation
Gradient system
Meridional current
Ocean currents
Pop-up
Functional stochastic differential equation
Tag
Time series
Trajectory
Zonal current

ABSTRACT

We consider some stochastic models that have been proposed for the trajectories of moving objects, including Brownian motion. This leads to the development of a general approach for dealing with paths including the use of functional stochastic differential equations. We then present an empirical example based on the surface drifting movements of a small satellite-linked radio transmitter tag after it detached from a whale shark in the western Indian Ocean. The daily estimates of the tag's locations were determined from transmissions received at irregular times by polar-orbiting satellites of the Argos Data Collection and Location Service system.

An aspect of the empirical analysis is a study of how well the sea surface currents that are derived from remote sensing and sea surface models compare to the movements of the drifting tag. A second is to develop a predictive model using the past tag locations, the currents and the winds.

1. Introduction

The study of trajectories has been basic to science for many centuries. It includes descriptions of the relative motions of planets, the movements of animals, and the routes of ocean transiting ships. More recently there has been considerable modeling and statistical analysis of biological and ecological processes of moving particles. These models may be formally motivated by difference and differential equations and by potential functions. Initially, following Liebnitz and Newton, they were described by deterministic differential equations, but variability around observed paths led to the introduction of stochastic models and corresponding calculi. Scientists, engineers, probabilists, and statisticians have been involved in the development. Other early researchers include Robert Brown, Bachelier, Einstein, Langevin, Wiener, Chandresekhar, and Ito. Their work led to the field of stochastic processes.

We have applied SDEs to describe the movements of northern elephant seals (Brillinger and Stewart, 1998) and elk (Brillinger et al., 2001). Stochastic gradient systems have been used in the case of monk seals (Brillinger et al., 2006, 2008) and the movements of a soccer ball during a game (Brillinger, 2007). Here we apply a functional stochastic differential equation (FSDE), sometimes called a stochastic functional differential equation, to the movement of a small radio transmitter drifting on the sea surface in the Indian Ocean.

* Corresponding author. Tel.: +1 510 642 0611; fax: +1 510 642 7892.
E-mail address: brill@stat.berkeley.edu (D.R. Brillinger).

0378-3758/$ - see front matter © 2010 Elsevier B.V. All rights reserved.
doi:10.1016/j.jspi.2010.04.026

There are three parts to this paper. The first presents some history and background theory, in seeking a unified approach to the problems. The second provides basic background concerning the derivation of current and wind values. The third focuses on the analysis of the movement of a small drifting satellite-linked radio transmitter tag, relative to ocean sea surface and wind currents, as it floated in the Indian Ocean after it detached from a whale shark that was tagged near South Ari Atoll in the Republic of the Maldives. There is an Appendix recording the result of Lai and Wei (1982) and a brief discussion of how it might be used.

The statistical methods that we use in the analysis include exploratory data analysis, regression analysis, stochastic differential equations and functional stochastic differential equations (FSDEs). Gradient systems are central. The models may be employed for forecasting future motion, e.g. when the tag is at location $r(t)$ at time t how well can its locations for the next 24 h be predicted? Also using simulation risk probabilities of interest, like the tag moving into some region of concern, can be estimated.

The data of primary interest are estimates of the tag's surface locations $\{r(t_i)\}$ at times $\{t_i\}$. The concern is the locations' dependences on explanatory variables like dynamic sea surface currents and winds and also the assessment of prediction models using past locations.

2. Modeling trajectories

2.1. History

In its beginning, the field of stochastic processes referred to realizations as paths or trajectories (e.g., Loeve, 1963, p. 500). As the field advanced, domains other than time became prominent. Since Newton's lifetime (1643–1727) equations of motion have typically been differential equations. With the advent of Brown's experiments, followed by the work of Bachelier, Wiener, Langevin, Chandresekhar, and Ito they became stochastic differential equations (SDEs). Deterministic expressions of Newton's equations can be written, in a common notation, as

$$\begin{aligned} v &= \mathrm{d}r/\mathrm{d}t \\ \mathrm{d}v/\mathrm{d}t &= -\beta v + X(r,t) \end{aligned} \tag{1}$$

with r position, v velocity, $-\beta v$ dynamical friction, and X acceleration (see Chandresekhar, 1943).

In some important cases, $X(r,t)$ has the form $-\mathrm{grad}\ \Phi(r;t)$ for some function, Φ (ibid expression 511). Here grad $X=(\partial\Phi/\partial x,\partial\Phi/\partial y)$.

The Smoluchovsky approximation

$$\mathrm{d}r/\mathrm{d}t = -\mathrm{grad}\ \Phi \tag{2}$$

follows by writing βX for X in (1) and assuming $|\beta|$large. The object of (1) becomes a *gradient system*, (Hirsch et al., 2004, p. 203). The structure $\mathrm{d}r/\mathrm{d}t$ is called a vector *field*. Its values are sometimes represented in figures as arrows superposed on a pertinent background. The function Φ is called a *potential*.

Working with a gradient system has advantages in statistical modeling for the potential function Φ is real-valued, as opposed to matrix and vector-valued β and X of (1).

Chandresekar (1943) also established equations of the form

$$\mathrm{d}v/\mathrm{d}t = -\beta v + X(r,t) + \mathrm{d}B/\mathrm{d}t$$

with v velocity, $\mathrm{d}B/\mathrm{d}t$ a noise-like process, β (a coefficient of friction) and X acceleration produced by an external force field. He referred to this equation as a generalized Langevin equation. Because of the presence of the random element $\mathrm{d}B/\mathrm{d}t$ it is an example of a stochastic differential equation (SDE).

Brownian motion refers to the movement of tiny particles suspended in a liquid. The phenomenon was named after Robert Brown, an Englishman who carried out detailed observations of the motion of pollen grains suspended in water, in 1827. It was later modeled by Einstein who was interested in the possibility that formalizing Brownian motion could support the theory that molecules indeed existed. Langevin (see Chandresekhar, 1943) established the following expression for the motion of such a particle:

$$m\,\mathrm{d}^2r/\mathrm{d}t^2 = -6\pi\mu a\,\mathrm{d}r/\mathrm{d}t + \mathrm{d}B/\mathrm{d}t$$

where r is location of a particle suspended in a liquid, m is the particle's mass, a is its radius, μ is the viscosity of the liquid, and $\mathrm{d}B/\mathrm{d}t$ is the "complementary force" (a noise-like term). This is a traditional example of an SDE. In practice the Ornstein–Uhlenbeck process is often referred to. It is given by

$$\mathrm{d}r(t) = Cr(t)\mathrm{d}t + \sigma\,\mathrm{d}B(t)$$

with C and σ constant matrices (see Bhattacharya and Waymire, 1990).

Functional stochastic differential equations, to be defined later, occur in the works of Ito and Nisio (1964) and Kubo (1966). Ito and Nisio set down the example

$$\mathrm{d}r(t) = \left[\mu + \int_{-\infty}^{0} r(t+s)\mathrm{d}A(s)\right]\mathrm{d}t + \mathrm{d}B(t)$$

in which the "velocity" $dr(t)/dt$ varies as a linear function of its previous locations. On the other hand Kubo (1966) considers a modified Ornstein–Uhlenbeck process represented by

$$dr = v\,dt$$
$$m\,dv = -m\left[\int_{-\infty}^{t} a(t-s)v(s)ds\right]dt + \sigma(r,v)dB$$

Initial conditions are now needed to complete the definition.

2.2. Concepts and notation

Notation employed here includes: time (t in R), location (r in R^p), Brownian (B in R^p), drift (μ in R^p), and diffusion (σ in $R^{p\times p}$). The concepts introduced will be used to describe and evaluate the movements of the drifting transmitter when $p=2$.

Potential function is a basic notion from Newtonian mechanics and leads directly to equations of motion in the deterministic case. The classic example of a potential function in R^3 is the gravitational potential. It is given by $\Phi(r) = -G|r-r_0|^{-1}$ with G the constant of gravitation (see Chandresekhar, 1943). This function leads to the attraction of a mass at position r towards the position r_0.

Considering stochastic concepts, the notion of a continuous time random walk can be formalized as Brownian motion. This is a continuous time process with the property that disjoint increments, $dB(t)$, are independent Gaussians with covariance matrix $I\,dt$, I the identity matrix. The random walk character becomes clear when one writes

$$B(t+dt) = B(t) + dB(t), \quad -\infty < t < \infty$$

which, anticipating what follows, can be written as

$$dr = dB$$

Following the work of Ito (1951) there has been extensive development of *stochastic differential equations* (SDEs). Ito used the notation

$$dr = \mu(r,t)dt + \sigma(r,t)dB \tag{3}$$

The process (3) is defined by converting the expression into an integral equation,

$$\int^t r(s)ds = r(t) = \int^t \mu(r(s),s)ds + \int^t \sigma(r(s),s)dB(s)$$

the integrals being defined as limits in mean square of the approximating sums.

The following discrete approximation, named after Euler and Maruyama, is useful. One writes

$$r(t_{i+1}) - r(t_i) = \mu(r(t_i),t_i)(t_{i+1}-t_i) + \sigma(r(t_i),t_i)\sqrt{\{t_{i+1}-t_i\}}\,Z_{i+1} \tag{4}$$

the $t_i \le t_{i+1}$ being points along the time line, and the Z_i independent standard multivariate normals. The square root in Eq. (4) results from the property that var $dB(t) = dt$ for standard Brownian motion. Expression (4) can be used to motivate likelihood-based statistical inferences.

It may be remarked that the notation for $r(\ )$ in (3) is in conflict with that just above; however, as will be seen, it is convenient to consider (4) as the model of record. Further, it is to be noted that (4) is now not considered as an approximation to the solution of (3), rather as stated it has become the model of record.

A *stochastic gradient system* is described via

$$dr = -\text{grad}\,\Phi\,dt + \sigma dB \tag{5}$$

for some differentiable $\Phi: R^2 \to R$ to be contrasted with (3).

Another concept, also associated with the name of Ito, is the *functional stochastic differential equation*. It has the form

$$dr = \mu(H(t),t)dt + \sigma(H(t),t)dB \tag{6}$$

with $H(t)$, the history $\{r(s), s \le t\}$ (for details see Ito and Nisio, 1964; Mao, 1997, 2003; Mohammed, 1984). The history $H(t)$ might consist of a single delayed term $r(t-S)$ for some $S > 0$ or an expression like $\int_0^S r(t-s)ds/S$. In fact in the work of this paper, and with $M(t)$ a cumulative count of the $t_j \le t$, we will employ

$$\mu(H(t),t) = \gamma \int_{t-1}^{t} r(s)dM(s)$$

for some constant γ.

A discrete version and approximate solution of the functional stochastic differential Eq. (6) is

$$r(t_{i+1}) - r(t_i) = \mu(H(t_i),t_i)(t_{i+1}-t_i) + \sigma(H(t_i),t_i)\sqrt{\{t_{i+1}-t_i\}}\,Z_{i+1} \tag{7}$$

where $H(t) = \{r(t_i), t_i \le t\}$ is the history up to time t, and with the Z_i independent standard multivariate normals. The square root term again results from the properties of Brownian motion. One reference is Ito and Nisio (1964). Other approximate solutions are available in Mohammed (1984) and Mao (1997,2003). When μ and σ are unknown, expression (7) leads to an approximation to the likelihood function and thereby large sample inference procedures.

We have previously applied SDEs to the movements of northern elephant seals (Brillinger and Stewart, 1998) and elk (Brillinger et al., 2001). Stochastic gradient systems have been used to model the movements of Hawaiian monk seals (Brillinger et al., 2008) and the movements of a soccer ball during a professional match (Brillinger, 2007). Another work is by Ionides et al. (2004) who studied cell motion.

Key features of the example of this paper are statistical dependence and irregularly spaced time points.

2.3. Statistical inference

A substantial literature is devoted to the topic of inference for stochastic differential equations (e.g., Basawa and Rao, 1980; Heyde, 1997). Interesting inference questions include: Is a particular motion Brownian? Is it Brownian with drift? Is it stationary? How does one predict future values? These can be formulated in terms of the functions μ and σ of (3) and (4).

Referring to (3) and (4), the estimation of a finite dimensional parameter can be carried out by ordinary least squares or maximum likelihood depending on the model and the distribution chosen for the Z_i. The naive approximation (4) is helpful for setting down approximate likelihood functions. The approximations can be anticipated to be effective if the time points, t_i, are reasonably close together. In a sense (4), not (3), has become the model of record. The works of Lai and Wei (1982) and Lai (1994) become useful in developing estimates and studying their properties.

Deciding on the functional form for the drift term μ and the diffusion coefficient σ is of concern. In Brillinger et al. (2001) the estimates considered are non-parametric and the generalized additive model is employed. Explanatories are included.

If the t_i are equally spaced, model (4) is a parametric or non-parametric stationary autoregression of order 1. It may be written as

$$y_{t+1} = \mu(y_t) + \sigma Z_{t+1}$$

t=1,2, … where μ and σ are parameters and the Z_{t+1} are independent and identically distributed (cf. Robinson, 1983; Hardle and Tsybakov, 1997; Hardle et al., 1998; Neumann and Kreiss, 1998). The quantities appearing may be vector-valued.

The NARX model (see Lai, 1994) may also be mentioned. It has the form

$$y_{t+1} = \mu(y_t,\ldots,y_{t-p}; x_{t-d},\ldots,x_{t-d-q}; \theta) + \varepsilon_{t+1}$$

with $\{\varepsilon_{t+1}\}$ a martingale difference sequence, $d \geq 1$ a delay, and θ a finite dimensional parameter to be estimated. In an extension model (7) may be written as

$$r(t_{i+1}) - r(t_i) = \mu(H(t_i), t_i; \theta)(t_{i+1} - t_i) + \sigma(H(t_i), t_i; \theta)\sqrt{\{t_{i+1} - t_i\}}\, Z_{i+1}$$

This gives an indication of the direction in which the practical work of this paper is heading.

3. Currents and winds

3.1. Atmosphere–ocean dynamics

The datum that we are concerned with is the sequence of locations of a small free floating transmitting tag and its dependence on dynamic sea surface currents and winds. The north–south and east–west currents are called the meridional and zonal, respectively. These may be estimated from the sea surface topography. The estimates may be improved by including sea surface wind and temperature. The sea surface height (SSH) may be estimated via satellite altimetry and then processed to obtain current estimates.

One derivation may be described as follows. The equation

$$\text{if } U_0 = -g \operatorname{grad} \zeta + A\tau + B \operatorname{grad} \theta \tag{8}$$

is developed in Bonjean and Lagerloef (2002). It is written employing complex-valued quantities. Here U_0 represents the surface current velocity, ζ denotes the deviation of the sea surface height at a given location and time from a long term level, τ represents surface winds, and θ, sea surface temperature. These are functions of both time and location. Continuing i is the square root of -1, the constants f and g are the Coriolis parameter and the acceleration due to gravity, respectively. A and B are multipliers involving depth. The first two terms on the right of (8) provide the geostrophic equations

$$U_y = f^{-1} g\, \partial\zeta/\partial x, \quad U_x = -f^{-1} g\, \partial\zeta/\partial y \tag{9}$$

with U_x and U_y as the east–west and north–south components of velocity, respectively. One sees that the desired currents may be estimated from the gradient of the sea surface height.

There are a variety of books, papers, and websites devoted to this topic. These include Gill (1982), Lagerloef et al. (1999), and Bonjean and Lagerloef (2002). Polovina et al. (1999) provide an application to model the movement of lobster larvae.

3.2. The drifting whale shark tag study

A pop-up archival tag (PAT; manufactured by Microwave Telemetry, Columbia, Maryland, USA) was attached to a whale shark (*Rhincodon typus*) near South Ari Atoll in the Republic of the Maldives on 13 May 2008 (Stewart et al., 2008). It remained attached to the shark until around 4 June 2008 when it detached, floated to the sea surface and then began transmitting to polar-orbiting satellites in the Argos Data Collection and Location Service (DCLS) system and continued until the batteries expired on 28 June.

The tag weighed about 65 g, measured about 33 cm long (including a 17 cm wire antenna), and was 2 cm in diameter with a small (4 cm diameter $\times$ 5 cm height) buoyant float at the base of the antenna. These tags are designed to collect and store measurements of hydrostatic pressure, water temperature, and ambient light levels at programmed intervals. Once the tag detaches from an animal, either at a programmed time or because the tag remains at constant depth for several days or approaches crush depth of the small buoyant float, it floats to the sea surface and then begins to continually transmit the stored data to the several polar-orbiting satellites in the Argos DCLS system. This continues until the tag's batteries expire. Those data are subsequently reported to researchers by daily emails or periodic electronic summary files. The movements of the shark while the tag was attached are then determined from the archived light level data (cf. Stewart and DeLong, 1995), diving patterns from the archived data on hydrostatic pressure, and thermal habitats from the archived data on water temperature.

In contrast, while the tag is drifting and transmitting data, its location is determined up to several times each day by the Argos DCLS from Doppler-shifts in the reception of two or more transmissions by an orbiting satellite. The accuracy of each location is estimated by the Argos DCLS based on a number of variables (cf. Stewart et al., 1989). For the comparisons that we make in this study, we used only those locations estimated to be 1 km or closer to the tag's likely true location (i.e., LC $\geq$ 1; see Stewart et al., 1989; Wilson et al., 2007).

During the 25 days that we tracked the drifting tag, we obtained 272 locations of LC $\geq$ 1.

Our goal here is to compare the movements (direction and velocity) of the drifting tag with the direction and velocity of sea surface currents that were estimated independently from remotely sensed data on sea surface height.

We assumed that the movements of the drifting tag would be influenced predominantly if not solely by sea surface currents owing to the *de minimus* size and mass of the transmitter and its small float. Our interests are in using this drift study as a null model to later examine the null hypothesis that movements of whale sharks are congruent with sea surface currents (i.e., a passive drifting movement model) using the remotely sensed data on sea surface currents as a key, accurate explanatory variable.

We downloaded Jason-1 data on estimated sea surface currents from the Ocean Watch Demonstration Project's Live Access Server $<$http://las.pfeg.noaa.gov/oceanWatch/oceanwatch.php$>$. The currents there were based on sea surface height deviation. The final values were a 10-day composite, the satellite taking 10 days to complete a cycle. The latitude and longitude resolutions were each 0.25°.

4. Results

4.1. Analysis of the motion

The first figure is a snapshot showing the currents on 4 June 2008 as arrows giving direction and speed (Fig. 1). The area shown runs from 72° to 82° east longitude and from 2° to 6° north latitude. The background is the bathymetry (i.e., ocean floor topography in meters of depth from the sea surface). The yellow vertical strip on the left represents the Chagos-Laccadive Ridge, where the Maldives Archipelago is located. The capitol city (Male) of the Republic of the Maldives is indicated. The yellow semicircle at the top right is shallow water leading into Sri Lanka.

The predominant water motion in this region is the Equatorial Countercurrent moving from west to east. However there is a lot of regional structure to that current owing to local eddies so that it is temporally and geographically dynamic. The black dot at about (74°E, 6°N) is where the satellite tag first appeared (i.e., popped up).

Fig. 2 provides the snapshot for the final day of data, 28 June. The continuous curve in the figure shows the tag's total observed track. The vector field provides the currents for 28 June.

The complete sequence of the daily figures, running from 4 to 28 June (missing June 15), may be found in Appendix B in the web version of this article.

The pdf file there may be paged through to follow the location of the drifting tag against a changing vector field of sea surface currents.

Referring to the sequence of pdf images the tag first appeared to behave according to the predominant driving forces of surface current. The odd and interesting event is on day 14 when the tag leaves the dominant current flow and enters a weak cyclonic eddy. It then moves slowly within that eddy until day 25 when a stronger southward flowing surface current begins to influence it. Had the tag not become temporarily trapped in this weak flowing eddy, on the basis of the currents we would have predicted that the tag should have continued to drift northeast and then eastward to wind up several hundred kilometers from where it did appear when the tracking ended. This appears to be a key change in state of expected movement from the hypothesis that movements are congruent with sea surface currents.

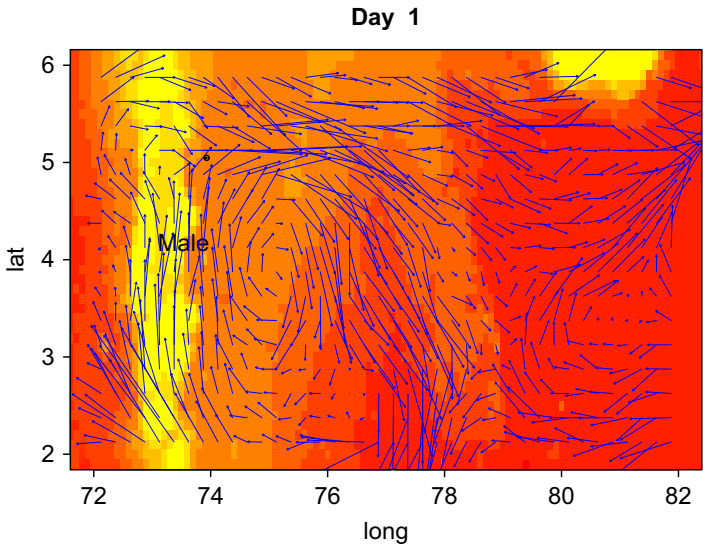

Fig. 1. Plot of estimated daily location of the drifting tag above a vector field of geostrophic currents with the background bathymetry. Yellow is shallowest and red deepest. "Day 1" refers to 4 June 2008 data. (For interpretation of the references to color in this figure legend, the reader is referred to the web version of this article.)

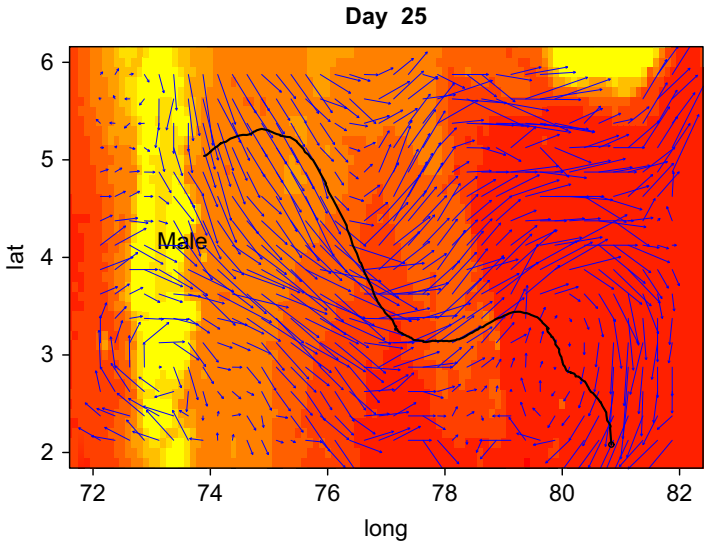

Fig. 2. Plot of estimated daily location of the tag above a vector field of geostrophic currents. "Day 25" refers to 28 June 2008.

The change around day 14 might be explained by some substantial, but small scale, brief but intense local sea surface or wind pattern events that perhaps became trivialized by the grosser scale 10-day measurement interval.

4.2. *The tag velocity*

Next consideration turns to comparisons of the tag currents with the satellite derived ones. The tag current at location $r(t_i)$ and time t_i was computed as

$$(r(t_{i+1})-r(t_i))/(t_{i+1}-t_i) \tag{10}$$

These tag values were at irregular times, but available several times daily. The satellite-determined current values were available only daily and are spaced 24 h apart. To have a direct comparison the satellite values were interpolated to obtain values at the tag times.

For the following computations, the effects of the outliers were reduced by applying a 5-day running biweight (see Mosteller and Tukey, 1977) to the values (10). Also the locations considered were those with LC >1.

Fig. 3 shows the biweighted tag velocities against time. The zonals are graphed as black lines in the two panels of Fig. 3. The top panel refers to the zonal case and the lower to the meridional. The red curves are satellite produced ones looked up along the track of the tag. The tag cases considered are those with the quality factor LC >1.

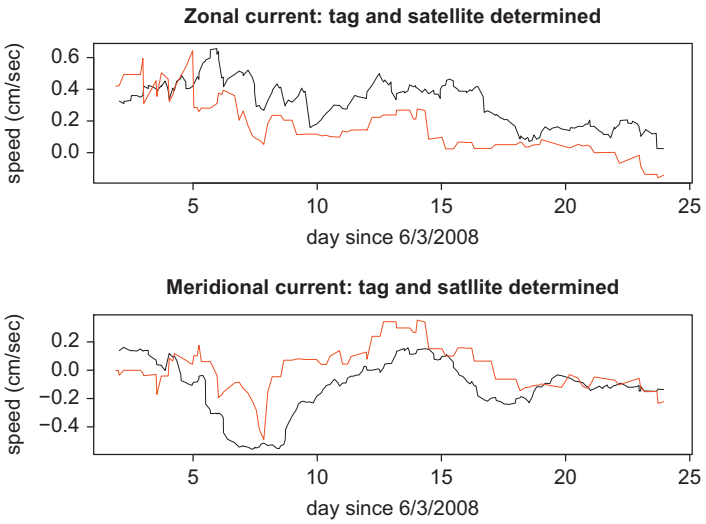

Fig. 3. The black lines provide the biweighted tag values (10). The top panel provides the east–west, i.e. zonal current and the bottom for the north–south, i.e. meridional. The red lines provides the geostrophic current values. (For interpretation of the references to color in this figure legend, the reader is referred to the web version of this article.)

The two curves in each panel are seen to follow each other to an extent with a slight amount of crossover, occurring near the beginning. The top panel of Fig. 3 indicates that the satellite zonal values are below the tag values much of the time. In the meridional case one notes that the tag ones stay lower longer for days 7–9 compared to the satellite based one. The correlation of the two curves in the top panel is 0.662 while in the bottom panel the correlation is 0.595. Sudre and Morrow (2008) remark on finding the correlation between satellite derived currents and drifter currents to be in the range 0.6–0.8 for most oceans. Lagerloef et al. (1999) refer to the ranges 0.4–0.9 for zonal and 0.0–0.7 for meridional currents. Note that these researchers report correlations, i.e. are allowing a location and scale transformation in their evaluation.

4.3. A stochastic model

Consider the stochastic gradient model, (5),

$$\mathrm{d}r = -\mathrm{grad}\,\Phi\,\mathrm{d}t + \sigma\,\mathrm{d}B.$$

It has the discrete approximation

$$(r(t_{i+1})-r(t_i))/(t_{i+1}-t_i) = v_{i+1} = \alpha+\beta X_C(r(t_i),t_i)+\sigma Z_{i+1}/\sqrt{(t_{i+1}-t_i)} \tag{11}$$

with $X_C(r,t)$ the 2×1 gradient vector at location r, and time t. In the present case X_C will be the geostrophic currents and Φ the sea surface height potential. These were shown in Fig. 3 as red curves. The −2 loglikelihood function corresponding to (11) is

$$\Sigma_i \left| v_{i+1}-\alpha-\beta X_C(r(t_i),t_i)\right|^2 (t_{i+1}\text{-}t_i)/\sigma^2$$

with v_{i+1} the velocity indicated in (11). In the zonal case the estimates of α and β are both substantially different from 0, assuming the errors, Z_{i+1}, to be independent standard bivariate normals. One is led to least squares as an estimation procedure. If estimation is by least squares and a large sample distribution is acceptable for the work then, following a theorem of Lai and Wei (1982), given in the Appendix, the Z_i do not have to be normal but simply independent to obtain useful approximations.

Note that the biweight values and the weights $(t_{i+1}-t_i)$ are employed in the following fittings. The proportion of variance explained is 0.460 for model (11) for the east–west motion. The meridional estimates are also substantially different from 0 with proportion of variance explained of 0.334.

Surface winds may be introduced into the model by including a term X_W

$$(r(t_{i+1})-r(t_i))/(t_{i+1}-t_i) = \alpha+\beta_C X_C(r(t_i),t_i)+\beta_W X_W(r(t_i),t_i)+\sigma Z_{i+1}/\sqrt{(t_{i+1}-t_i)} \tag{12}$$

The wind values were obtained from the Ocean Watch Demonstration Project's Live Access Server. When this enlarged model is fit the proportions of variance explained become 0.537 and 0.624 for the zonal and meridional cases, respectively. These values may be compared with the preceding 0.460 and 0.334 and appear substantially larger. The significance levels of the estimates of the coefficients β_C and β_W were both high, under Gaussian and independence assumptions. The standard errors computed may be justified by the work of Lai and Wei (1982) (see Appendix A).

The figure shows a pattern remaining in the residuals. It might be that this was introduced by the interpolation, but when simply the 24 daily values were employed the results' character remained much the same as in Fig. 4. The winds

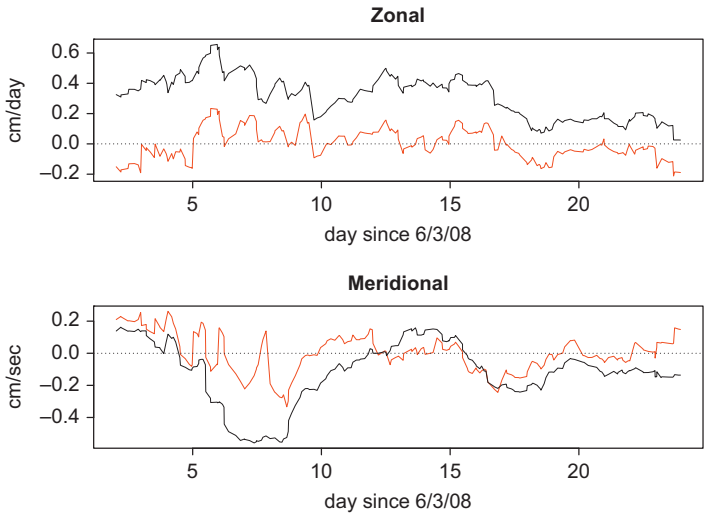

Fig. 4. Tag based values are in black. Residuals from fitting current and wind are in red. (For interpretation of the references to color in this figure legend, the reader is referred to the web version of this article.)

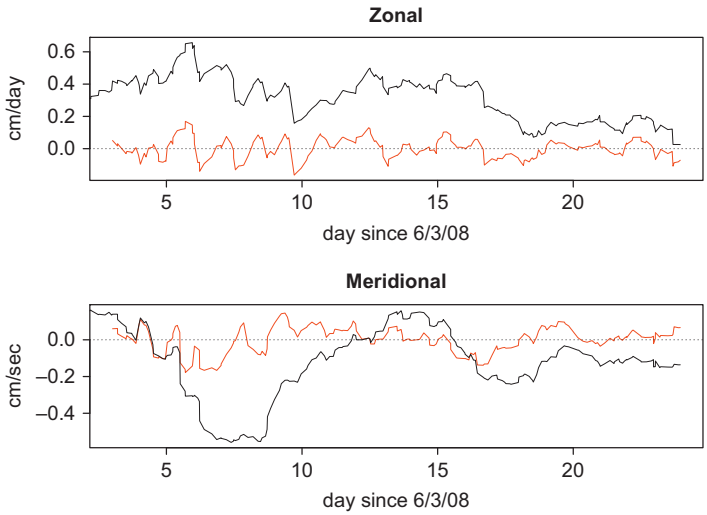

Fig. 5. Results of fitting model (12) (i.e. including current, wind, and average of locations for the tag during the preceding 24 h).

downloaded were on a slightly different grid, so some interpolation was necessary to put them on the same scale as the current values.

To study this situation further a functional stochastic differential equation was set up. That model is

$$(r(t_{i+1})-r(t_i))/(t_{i+1}-t_i)=\mu(H(t_i),t_i)+\alpha+\beta_C X_C(r(t_i),t_i)+\beta_W X_W(r(t_i),t_i)+\sigma\sqrt{Z_{i+1}}/\sqrt{\{t_{i+1}-t_i\}} \tag{13}$$

with

$$\mu(H(t),t)=\gamma\int_{t-24}^{t} r(s)dN(s)/[N(t)-N(t-24)] \tag{14}$$

i.e. γ times the mean of the $r(t_j)$ values over the immediately preceding 24 h period. The reason for this step was that the residual plots of the preceding model fits provided evidence for the presence of remaining temporal dependence. The added term could deal with it.

Fig. 5 provides plots of the biweighted tag velocities in black and the residual series in red from modeling the tagged cases as a function of the corresponding satellite current values, wind values and the tags mean location during the preceding 24 h.

The amount of variability explained increased further. In the zonal case the proportion goes from 0.460 when currents only are fitted to 0.537 when winds are added and then to 0.804 when the previous 24 h values are brought in. In the meridional case it goes from 0.334 when currents only are fitted to 0.624 when winds are added and then to 0.853 when the previous 24 h values are brought in. The parameter γ was defined via expression (14).

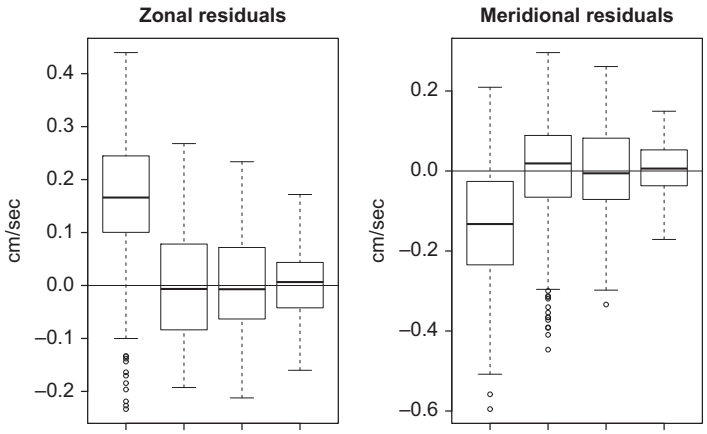

Fig. 6. Parallel boxplots of residuals resulting from predicting the observed tag velocity by the sequence of models described in the text.

Estimated regression coefficients, standard errors, and *t*-values follow.

Zonal case			
γ	0.742828	0.051252	14.494
β_C	0.201452	0.039224	5.136
β_W	−0.009115	0.003862	−2.360

Multiple *R*-squared: 0.804.

Meridional case			
γ	0.708062	0.041549	17.042
β_C	0.240575	0.039707	6.059
β_W	0.025608	0.005453	4.696

Multiple *R*-squared: 0.854.

One notes that the *t*-statistics are each substantial. All three of the explanatories enter into the fitted model.

The improvements resulting from successively expanding the model are summarized by parallel boxplots in Fig. 6. Case 1 refers to predicting the tag velocity simply by the NOAA current based one. Case 2 refers to regressing the tag velocity on the NOAA one as in model (11). Case 3 adds the wind and case 4 further adds the average position of the available ones for the preceding 24 h as in models (12) and (13).

One sees the spread decreasing and the distribution becoming more symmetrical as variables are added.

Expression (13) provides a means of predicting the future locations of the tag using the currents, the winds, and an average of the preceding past locations.

5. Summary and discussion

In preparation for analyses and further studies of movements of tagged whale sharks, we initiated this study of a freely floating tag. Two classes of data were collected, both involved satellite measures. One, the currents had to be inferred via a gradient computation, and the other, the estimated tag velocity was a numerical derivative. A fundamental model was set up in continuous time via a stochastic differential equation. Then there was a switch to a numerical form recognizing the character of the actual data. Estimation of the currents led to a gradient system. Developing a succession of regression-like models led to a functional stochastic differential equation involving past positions of the tag in its description.

Robust methods were basic because of the presence of outliers.

In conclusion it seems that both the current and wind measurements will be useful, but their error needs to be further understood. The paper may be viewed as a progress report, particularly since Ocean Watch Demonstration Project's current estimates employed are not viewed as being of "science-quality", i.e. refinements have been developed but not implemented.

Acknowledgements

Manny Parzen once asked DRB, "What is the cat always thinking?" Manny's answer, "What have you done for me lately?" Well Manny, I am so often thinking that you have done so much for my family and me both a long time ago and lately. Thank you so much.

The work was supported by the NSF Grant DMS-0707157 and by funding to B.S. Stewart by the Kerzner Marine Foundation and the Hubbs-SeaWorld Research Institute. We thank M. Riley, R. Rees, R. Lloyd-Williams, and Adam Harmon for their collaboration during tagging studies of whale sharks in the Maldives, Conrad Rengali, M. Faiz, A. Naseer, M. Shiham Adam, C. Anderson, and M. Hameed for their support and facilitation of the work in the Maldives, Cindy Bessey, Lynn Dewitt, Dave Foley, and Roy Mendolssohn for their comments and suggestions on oceanographic data, Charlotte Wickham for comments on a draft of the paper, and the referees.

The tagging research program was authorized under Marine Research Permit No. IR-P/2008/03 from the Ministry of Fisheries, Agriculture and Marine Resources (Male, Republic of Maldives).

Appendix A

Theorem A1. Lai and Wei (1982). Consider the regression model

$$y_i = x_i^T \beta + \varepsilon_i$$

i=1,2, … with $\{\varepsilon_i\}$ martingale differences with respect to an increasing sequence of σ-fields $\{F_n\}$. Suppose that $\sup_n \mathrm{E}(\|\varepsilon_n\|^{\alpha}|F_{n-1}) < \infty$ a.s. for some $\alpha > 2$. Suppose further that $\lim_{n\to\infty} \mathrm{var}\{\varepsilon_n|F_{n-1}\}=\sigma^2$ almost surely for some nonstochastic σ. Assume that x_n is an F_{n-1}-measurable random variable and that there exists a non-random positive definite symmetric $L \times L$ matrix B_n for which

$$B_n^{-1}(X_n{}^T X_n)^{1/2} \to I \tag{14}$$

and $\sup_{1 \le i \le n} \|B_n^{-1} x_n\| \to 0$ in probability. Then

$$(X_n^T X_n)^{1/2}(b-\beta) \to N(0,\sigma^2 I)$$

in distribution as $n \to \infty$.

Note that 0 means independent observations like the $\sigma \mathbf{Z}_{i+1}$ of (14) form a martingale difference sequence with respect to the σ-field F_i generated by $\{r(t_1), \ldots, r(t_i)\}$.

Justifying the assumption (14) may follow in the manner of Brillinger (1973).

Theorem A2. Under the assumptions of Theorem A1 and $\lim \log \lambda_{\max}(X_n^T X_n)/n \to 0$ almost surely, one has

$$((\varphi(r)(X_n^T X_n)^{-1}\varphi(r)^T)^{-1/2}\varphi(r)^T(b-\beta)/s_n \to N(0,1)$$

in distribution as $n \to \infty$.

The additional assumption in Theorem A2 is to have the almost sure convergence of s_n to σ.

Appendix B. Supplementary data

Supplementary data associated with this article can be found in the online version at doi:10.1016/j.jspi.2010.04.026.

References

Basawa, I.V., Rao, Prakasha, 1980. In: Statistical Inference for Stochastic Processes. Academic, London.
Bhattacharya, R.N., Waymire, E.C., 1990. In: Stochastic Processes with Applications. Wiley, New York.
Bonjean, F., Lagerloef, G.S.E., 2002. Diagnostic model and analysis of the surface currents in the Tropical Pacific Ocean. J. Phys. Oceanogr. 32, 2938–2954.
Brillinger, D.R., 1973. Estimating the mean of a stationary time series by sampling. J. Appl. Probab. 10, 419–431.
Brillinger, D.R., 2007. A potential function approach to the flow of play in soccer. J. Quant. Anal. Sports January.
Brillinger, D.R., Preisler, H.K., Ager, A.A., Kie, J.G., 2001. The use of potential functions in modelling animal movement. In: Saleh, A.K.M.E. (Ed.), Data Analysis from Statistical Foundations. Nova Science, Huntington, pp. 369.
Brillinger, D.R., Stewart, B.S., 1998. Elephant seal movements: modelling migration. Can. J. Stat. 26, 431–443.
Brillinger, D.R., Stewart, B., Littnan, C., 2008. Three months journeying of a Hawaiian monk seal. Probability and statistics: essays in honor of David A. Freedman. Institute of Mathematical Statistics Collections. 2, pp. 246–264.
Brillinger, D.R., Stewart, B., Littnan, C., 2006. A meandering hylje. In: Liski, E.P., Isotalo, J., Puntanen, S., Styan, G.P.H. (Eds.), Festschrift for Tarmo Pukkila on his 60th Birthday. Department of Mathematics, Statistics and Philosophy, University of Tampere.
Chandrasekhar, S., 1943. Stochastic problems in physics and astronomy. Rev. Mod. Phys. 15, 1–89.
Gill, A.E., 1982. In: Atmosphere–Ocean Dynamics. Academic, San Diego.
Hardle, W., Tsybakov, A., 1997. Local polynomial estimators for the volatility function in nonparametric regression. J. Econometrics 81, 223–242.
Hardle, W., Tsybakov, A., Yang, L., 1998. Nonparametric vector autoregression. J. Stat. Plann. Inference 68, 221–245.
Heyde, C.C., 1997. In: Quasi-Likelihood and its Application. Springer, New York.
Hirsch, M.W., Smale, S., Devaney, R.L., 2004. In: Differential Equations, Dynamical Systems and an Introduction to Chaos second ed. Elsevier, Amsterdam.
Ionides, E.L., Fang, K.S., Isseroff, R.R., Oster, G.F., 2004. Stochastic models for cell motion and taxis. J. Math. Biol. 48, 23–37.
Ito, K., 1951. In: On Stochastic Differential Equations. American Mathematical Soc., Providence.
Ito, K., Nisio, M., 1964. On stationary solutions of a stochastic differential equation. J. Math. Kyoto Univ. 4, 1–75.
Kubo, R., 1966. The fluctuation–dissipation theorem and Brownian motion. In: Kubo, R. (Ed.), Many-Body Theory. Benjamin, New York.
Lagerloef, G.S.E., Mitchum, G.T., Lukas, R.B., Niiler, P.P., 1999. Tropical Pacific near-surface currents estimated from altimeter, wind, and drifter data. J. Geophys. Res. 104, 23313–23326.
Lai, T.L., 1994. Asymptotic properties of nonlinear least squares estimates in stochastic regression models. Ann. Stat. 22, 1917–1930.

Lai, T.L., Wei, C.Z., 1982. Least squares estimation in stochastic regression models with applications to identification and control of dynamic systems. Ann. Stat. 10, 154–166.
Loeve, M., 1963. Probability Theory. Van Nostram, Princeton.
Mao, X., 1997. In: Stochastic Differential Equations and Applications. Horwood, Chichester.
Mao, X., 2003. Numerical solutions of stochastic functional differential equations. London Math. Soc. J. Comput. Math. 6, 141–161.
Mohammed, S.-E.A., 1984. In: Stochastic Functional Differential Equations. Pitman, London.
Mosteller, F., Tukey, J.W., 1977. In: Data Analysis and Regression. Addison-Wesley, Boston.
Neumann, M.H., Kreiss, J.-P., 1998. Regression-type inference in nonparametric autoregression. Ann. Stat. 26, 1570–1613.
Polovina, J.J., Kleiber, P., Kobayashi, D.R., 1999. Application of TOPEX/Poseidon satellite altimetry to simulate transport dynamics of larvae spiny lobstster, *Panulirus marginatus*, in Nortwestern Hawaiian Islands. 1993–1996. Fish. Bull. 97, 132–143.
Robinson, P.M., 1983. Nonparametric estimators for time series. J. Time Ser. Anal. 4, 185–207.
Stewart, B.S., DeLong, R.L., 1995. Double migrations of the northern elephant seal, *Mirounga angustirostris*. J. Mammal. 78, 1101–1116.
Stewart, B.S., Leatherwood, S., Yochem, P.K., Heide-Jorgensen, M.-P., 1989. Harbor seal tracking and telemetry by satellite. Mar. Mammal Sci. 5, 361–375.
Stewart, B.S., Riley, M., Rees, R., Lloyd-Williams, R., Harman, A., 2008. Ecology of the whale sharks of the Republic of the Maldives. Hubbs-SeaWorld Research Institute Technical Report 2008, 363, pp. 1–17.
Sudre, J., Morrow, R.A., 2008. Global surface currents: a high-resolution product for investigating ocean dynamics. Ocean Dyn. 58, 101–118.
Wilson, S.G., Stewart, B.S., Polovina, J.J., Meekan, M.G., Stevens, J.D., Galuardi, B., 2007. Accuracy and precision of archival tag data: a multiple-tagging study conducted on a whale shark (*Rhincodon typus*) in the Indian Ocean. Fish. Oceanogr. 16, 547–554.